16th Australasian Fluid Mechanics Conference
Crown Plaza, Gold Coast, Australia
2-7 December 2007

Numerical Simulations of Flows over a Forced Oscillating Cylinder

T.T. Do[1], L. Chen[2] and J.Y. Tu[1]
[1] School of Aerospace, Mechanical and Manufacturing Engineering,
RMIT University, P.O. Box 71, Bundoora,, Vic. 3083, Australia
[2] Maritime Platform Division,
Defence Science & Technology Organisation, P.O. Box 4331, Melbourne, Vic. 3001, Australia

Abstract

A numerical study of incompressible laminar flow past a circular cylinder forced to oscillate longitudinally, transversely and at an angle to the uniform freestream is performed using the dynamic mesh method. The simulations are conducted at a fixed Reynolds number of 80 with amplitude ratios varying between 0.14 to 0.50 and excitation frequency ratios of 0.05 to 3.0. Good agreement to previous experimental and numerical investigations is achieved in the prediction of the lock-on range, force amplifications and vortex shedding modes for longitudinal and transverse oscillations. For excitations at an angle of 60 degrees relative to the oncoming flow, previously identified modes of AI and, AII were successfully predicted. In addition, at higher amplitude ratios the entire synchronised von Karman wake street displayed a deviating effect from the centreline. Analysis of the wake response via phase plane diagrams and the transverse force coefficients revealed two lock-on regions. The extents of these lock-on regions, and the variation of the forces and near wake vortex shedding modes are presented and discussed herein.

Introduction

Viscous flow over a controlled oscillating circular cylinder continues to attract much attention in both the academic and practical engineering arenas due to the rich blend of physics presented. This nonlinear flow, arising from the interaction of the fluid and the structure, is largely influenced by the combination of the oscillating amplitude ratio *A/D* and the excitation frequency ratio f_e/f_{s0} [[7],[12]], where *A, D,* f_e, and f_{s0} are displacement amplitude, cylinder diameter, excitation frequency and vortex shedding frequency of a stationary cylinder respectively. At the right combination, the flow may induce one or more fascinating and complex phenomena such as hysteresis, bifurcation, synchronisation and transformation or competition of the vortex shedding patterns [[2],[4],[13]]. These pose a great challenge to both theoretical and experimental fields.

Crossflow oscillations are commonly found in atmospheric flows around chimneys, transmission wires, high-rise buildings and suspension bridge cables. This has led to a significant number of experimental and numerical studies of circular cylinders undergoing forced transverse oscillations [[2],[9],[10],[11],[14],[17]]. Hence it is generally known that lock-on occurs within a small range of f_e/f_{s0} close to unity. In this lock-on range, Bishop & Hassan [1] observed an abrupt phase shift between the transverse force and cylinder displacement. Later, Tanida *et al.* [15] showed that the large scale vortex shedding frequency of the vibrating cylinder, f_s, is exactly equal to the excitation frequency, f_e i.e. $f_e/f_s = 1$.

Experimental studies of longitudinally forced cylinder oscillations are relatively less common compared to transversely forced excitations. Perhaps this is because the longitudinal fluctuating force F_x exerted on the cylinder is weaker, being only one tenth in magnitude of the transverse fluctuating force F_y [3]. Nonetheless, in hydrodynamic flows, this F_x component has been known to excite braced members of off-shore structures, marine piles and submarine periscopes [8], and is of engineering significance. Tanida *et al.* [15] revealed that lock-on occurs over the forcing frequency of $1.5 \le f_e/f_{s0} \le 2.0$ for *Re=80* with *A/D=0.14* for inline oscillations, and the large scale vortex shedding frequency of the vibrating cylinder is exactly one half of the excitation frequency i.e. $f_e/f_s = 2$.

Investigations of a circular cylinder experiencing forced oscillations at an angle α with respect to an incoming flow on the other hand have been rare. Öngören & Rockwell [13] examined such oscillations at 45° & 60° as well as performing longitudinal and transverse oscillations. They observed two main vortex shedding modes, symmetrical (S) and antisymmetrical (A), where the antisymmetrical mode is further sub-classified into AI, AII, AIII and AIV. Oscillations at 60° angle exhibit synchronized vortex shedding modes at $f_e/f_{s0} = 1$, $f_e/f_{s0} = 2$ and $f_e/f_{s0} \ge 4$ in the form of AI, AII and S respectively, while at other excitation frequencies, repeating occurrences of S and A modes were observed over time. However, only qualitative information from flow visualization can be found from their study and hence detailed lock-on flow regimes and analysis of the forces is not available. Questions also arise for the case of 60° excitations as to whether the vortex street wake may be modified when the circular cylinder is forced to oscillate at larger amplitude ratios.

Due to the well-known advantages of numerical methods, a significant number of computational studies have been conducted to study both inline and crossflow forced oscillations, most using methods different from the one adopted in this study [4]. In this numerical study, a commercially available code with the dynamic meshing feature is utilised to simulate the "physically" oscillating motion of the circular cylinder. This feature presents a powerful method in simulating a moving body in the presence of other structures. The objectives of this study are firstly to assess the capability of this dynamic mesh feature in modelling flows with fluid-structure interactions and, secondly, to provide an analysis of the fluctuating forces and identify the lock-on regimes for a circular cylinder oscillating longitudinal and transverse to the freestream direction with emphasis given to the case with 60° oscillations, which has fewer data available. The Reynolds number is fixed at 80 while the amplitude ratio and the excitation frequency are varied from 0.14-0.5 and 0-3f_{s0} respectively.

Modelling Procedure & Validation

All flows simulated in this study have a fixed Reynolds number of 80. Due to the low Reynolds number, the flow is considered laminar and two-dimensional. Figure 1 provides the details of a typical computational domain used in this study with the circular cylinder having a diameter of *D*=0.01m. Given the low Reynolds number, the vertical boundary located at *12D* should be sufficient far to implement the free-stream boundary conditions. It was found that a distance between the centre of the cylinder to the outlet equal to *4D* led to a discrepancy with the benchmark solution less than 15% [6]. In this study, this distance was *40D* that was larger than *25D* used in the benchmark solution [6].

Discretization was achieved using triangular cells everywhere except in the thin region enveloping the circular cylinder, where quadrilateral cells were designated up to a thickness of 0.1D to increase accuracy in resolving the boundary layer flows (see inset of Figure 1). The surface of the cylinder was defined with a no-slip *wall* boundary condition. The limits for either the "birth" or "death" of a grid cell for the dynamic meshing adaptation in terms of maximum cell skewness, minimum length scale and maximum length scale were limited to 0.6, 0.001D and 0.01D respectively. The segregated second-order implicit unsteady solver approach was selected together with the SIMPLE method to achieve pressure-velocity coupling. The scheme used was first-order accurate in the time domain while second-order accurate in the spatial domain.

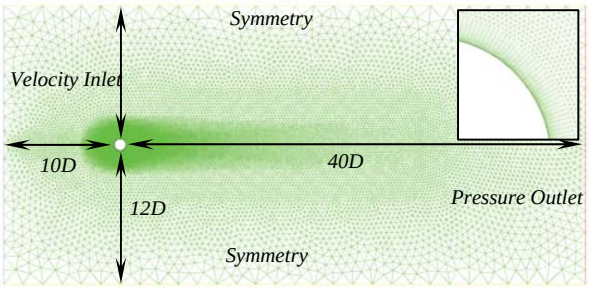

Figure 1 - Details of a typical two-dimensional computational domain.

Two meshes A and B were developed for grid independence analysis and validation. Mesh A and B have 41,510 and 57,704 cells respectively. The influent of time steps on the solution was investigated. It was found that a time-step independent solution was obtained at $\Delta t = 0.0025$. Table 1 provides the comparison of the Strouhal number (*St*), mean longitudinal force coefficient C_x and the peak-to-peak values of transverse force coefficient C_y of the two meshes. The results were for flow past a stationary circular cylinder with a Reynolds number of 100.

	St	$\overline{C_x}$	***C_y Peak-to-Peak***
Mesh A	0.1657	1.356	0.603
Mesh B	0.1635	1.357	0.604
Tritton [16]	0.15-0.18	1.26-1.32	---
Braza et al. [5]	0.16	1.3	0.6
Li et al. [11]	0.176	1.333	0.685

Table 1 – Comparison of main flow characteristics with published data for flow past a stationary cylinder with *Re*=100.

Table 1 shows that the solutions of the two meshes have converged, hence grid independence was achieved. Comparison of the main flow characteristics shows excellent agreement with the published data. The denser mesh, Mesh B, was used throughout this numerical simulation to ensure adequate cells to account for the death and birth of cells in the dynamic re-meshing process.

Results and Discussions

The motion due to forced oscillation of a circular cylinder at an arbitrary angle α relative to the oncoming flow is depicted in Figure 2. (The relative displacement shown here is grossly exaggerated for clarity.)

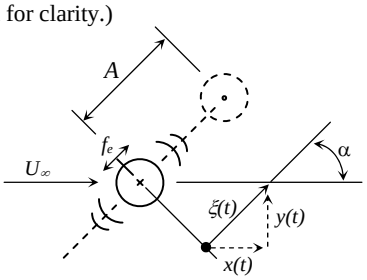

Figure 2 – Circular cylinder undergoing forced oscillations at an angle with respect to oncoming flow.

The maximum displacement amplitude is *A* and the trajectory of the rigid cylinder at time *t* is given as *ξ(t)*. For harmonic sinusoidal motion of the cylinder, *ξ(t)* is defined as:

$$\xi(t) = A\sin(2\pi f_e t) \quad (1)$$

Using the Cartesian coordinates to describe the motion of the cylinder and keeping the oscillations in a straight line i.e. $fe_x = fe_y = fe$ we have:

$$x(t) = [A\cos(\alpha)]\sin(2\pi f_e t) \quad (2)$$

$$y(t) = [A\sin(\alpha)]\sin(2\pi f_e t) \quad (3)$$

Equations 2 & 3 are used to specify the periodic oscillations of the cylinder.

Transverse oscillations (α=90°)

A comparison of the excitation vortex shedding frequency ratio (f_e/f_s) with an experimental study by Tanida *et al.* [15] and a numerical simulation by Patnaik *et al.* [14] is shown in Figure 3. The lock-on frequency range predicted by the current study is $0.82 \le f_e/f_{s0} \le 1.07$, which is seen to slightly under-predict the experimental results. On the other hand, it is more consistent with the numerical investigation by Patnaik *et al.* [14]. Figure 3 also shows the time averaged longitudinal force coefficient $\overline{C_x}$ across the forcing frequency range compared to experimental data. A good agreement of $\overline{C_x}$ values with experimental data is achieved outside the lock-on range. Within the lock-on region the numerical results showed an under-prediction of $\overline{C_x}$ around 10%, although the forcing frequency ratio at which the peak of $\overline{C_x}$ occurs corresponds well to experimental results. Moreover, Bishop & Hassan [3] showed that in the lock-on state the longitudinal force is amplified. By assessing the experimental results of $\overline{C_x}$ and f_e/f_s curves in Figure 3, it is seen that amplification range of $\overline{C_x}$ does not conform to that of the lock-on range revealed by f_e/f_s. The beginning and the end of the force variation region is approximately at $f_e/f_s = 0.77$ and $f_e/f_s = 1.16$ respectively, whereas the start and the end of the lock-on region is $f_e/f_s = 0.64$ and $f_e/f_s = 1.28$. The narrower $\overline{C_x}$ amplification region from the experimental results might suggest that the lock-on region could be shorter, which agrees with the predictions of the current computations and that of Patnaik *et al.* [14]. The vortex shedding pattern of forced transverse oscillations within the current parameters was in the form of the regular von Karman street wake. At lock on, the previously identified antisymmetrical AI mode [13] or the equivalent 2S mode [17] was observed (not shown).

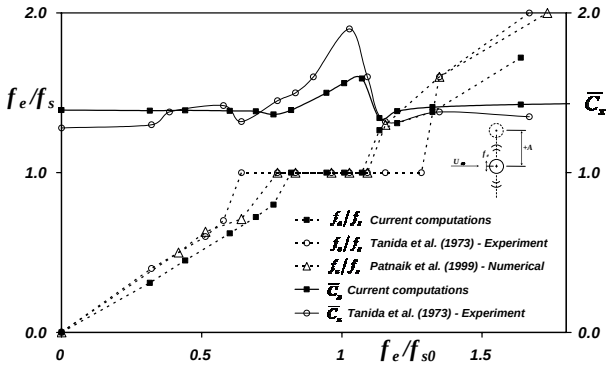

Figure 3 – Vortex shedding frequency ratio and mean longitudinal force coefficient variation compared with published data, *Re=80, A/D=0.14*.

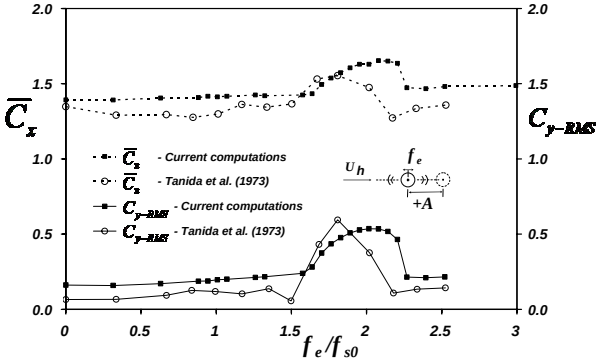

Figure 5 – Mean longitudinal force coefficient and root-mean-square of transverse force coefficient compared with experimental data for inline oscillations, *Re=80, A/D=0.14*.

Longitudinal oscillations (α=0°)

For forced inline oscillations, the ratio of the excitation frequency to the large scale vortex shedding frequency (f_e/f_s) is exactly 2 in the lock-on state as shown in Figure 4. A comparison of f_e/f_s throughout the excitation frequency ratio in Figure 4 showed the current computation satisfactorily matched that of the experimental data performed by Tanida *et al.* [15]. However, the lock-on region was predicted at higher excitation frequencies, corresponding to shifting the lock-on range to the right. The lock-on range of the experimental data reported was $1.5 \le f_e/f_{s0} \le 2$ while the result from the current computation is $0.64 \le f_e/f_{s0} \le 2.21$. Figure 5 provides a comparison of the mean longitudinal force coefficient and root-mean-square of the transverse force coefficient to experimental data also by Tanida *et al.* [15]. It is apparent that in the lock-on state, there is a substantial amplification of both the longitudinal and the transverse forces on the cylinder. Figure 5 also shows a reasonable agreement is achieved for both force coefficients, although $\overline{C_x}$ is noticeably over-predicting the experimental data at higher f_e/f_s. The discrepancy could be due to the well known fact that it is difficult to measure the longitudinal force, which is significantly less than that of the transverse force, especially for low Reynolds number flows.

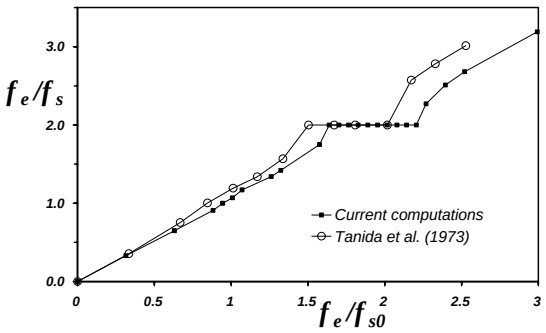

Figure 4 – Comparison of lock-on region for inline forced oscillations, *Re=80, A/D=0.14*.

In contrast to the forced transverse oscillation, where only one synchronised mode of vortex shedding was observed, the longitudinal forced oscillation exhibits several distinct modes in the near wake. Outside the lock-on range, the vortices are shed in an irregular manner, resulting in a disorderly wake. At lock-on, two definite synchronised modes, the so called 2P-per-2T and 2S-per-2T mode are observed at the lower lock-on end ($f_e/f_s = 1.64$) and the upper lock-on end ($f_e/f_s = 2.21$) respectively. In the 2P-per-2T mode, a pair (P) of vortices is shed on each side of the circular cylinder per two periods (T) of oscillation, while 2S-per-2T mode corresponds to two single (S) vortices being shed in two periods of oscillation on each side of the circular cylinder. Figure 6 illustrates these two modes. At the lower excitation frequency of $f_e/f_s = 1.64$, the vorticity ceases to feed into the growing vortex at the end of each forward stroke (cylinder moving left to right), and hence it is shed downstream. As the cylinder undergoes the backward stroke a new vortex starts to form, however due to the low frequency and hence speed, the rate at which the second vortex forms is slow, allowing the previous vortex to convect a good distance downstream. This causes two distinct vortices to shed on each side of the cylinder before coalescing into one vortex at approximately 6D downstream (Figure 6, column (a) at 1.0T). For higher excitation frequency ($f_e/f_s = 2.21$), the same process applies, only due to the now faster oscillating speed causing the second vortex to "catch-up" with the first vortex and promptly coalescing into a single vortex producing a 2S-per-2T mode as seen in Figure 6, at 1.5T.

These 2P-per-2T and 2S-per-2T modes are equivalent to AIV and AII respectively, according to the mode classification by Öngören & Rockwell [13]. The current observation is in agreement with a recent numerical study with $\mathrm{Re} = 200$ and $A/D = 0.1$ by Al-Mdallal *et al.* [1]. However, Öngören & Rockwell [13] observed an AIII mode for $\mathrm{Re} = 855$ and $A/D = 0.13$ in the lock-on range for longitudinal oscillations, where the AIII mode consists of two counter-rotating vortices followed by a single vortex in every two periods of oscillations. The disagreement could be due to the much higher Reynolds number in the experiment performed by Öngören & Rockwell [13].

Increasing the excitation frequency ratio to $f_e/f_s = 3$, a symmetric vortex shedding mode was achieved as shown in Figure 7. A persistent and simultaneous shedding of one single vortex on each side of the circular cylinder is observed for every one period of oscillation. The symmetry feature is highly unstable and quickly become influenced by the local flow whereby one vortex of the preceding symmetrical pair gets drawn

back to coalesce with the forming vortex pair. The current prediction of the symmetric vortex shedding mode is consistent with the flow visualization of Öngören & Rockwell [13] at the same excitation frequency ratio. However, in their experimental investigation the symmetrical vortices pertained up to three vortex pairs downstream of the cylinder. Again this could possibly due to the much higher Reynolds number (*Re=855*).

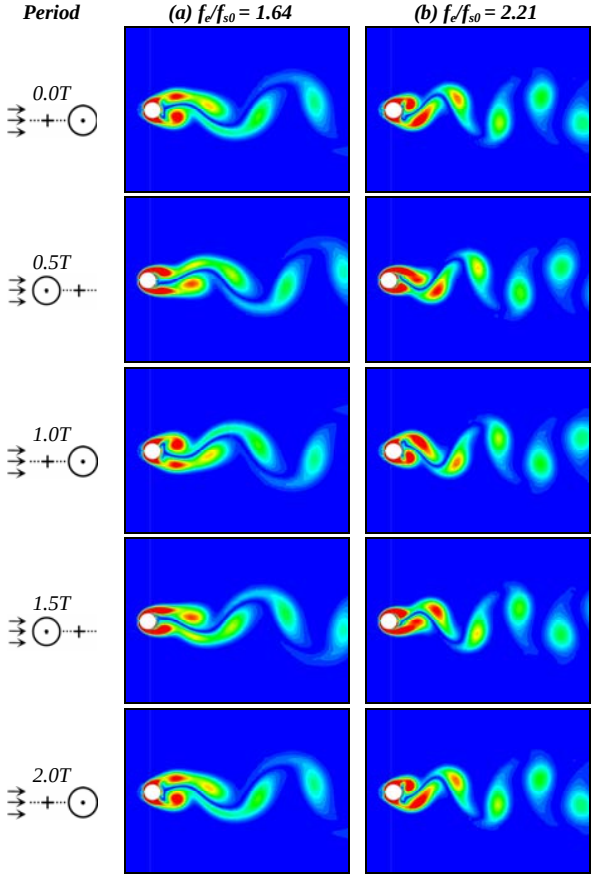

Figure 6– Instantaneous vorticity contours for 2 periods (2T) of longitudinal oscillations illustrating (a) 2P-per-2T mode and (b) 2S-per-2T mode.

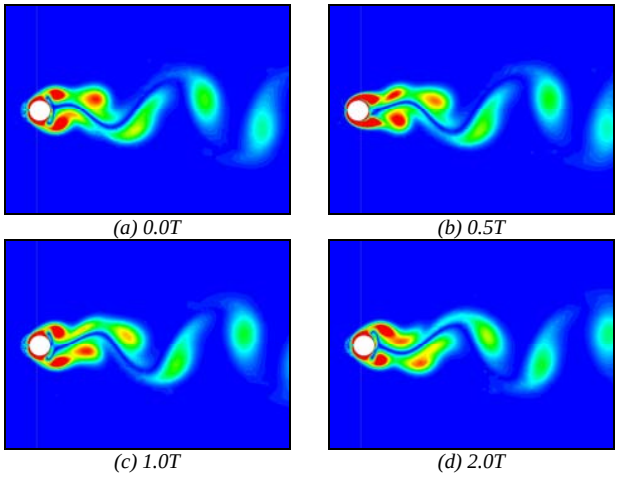

Figure 7 – Near wake symmetric vortex shedding for longitudinal oscillations at $f_e/f_s = 3$ in two periods of oscillations.

Oscillations at α=60°

When the circular cylinder is forced to oscillate at an angle of 60° with respect to the oncoming flow, it experiences both inline and transverse excitation modes. In conjunction with application of classical spectral density analysis to extract the embedded frequencies, Lissajous figures or phase-plane diagrams were also employed to identify the lock-on states, following Koopman [9], Karniadakis & Triantafyllou [7], Li *et al.* [11] and Patnaik *et al.* [14]. The present study used the longitudinal velocity (u_x) and transverse velocity (u_y) as the two independent variables of the system, plotted continuously over time. For each excitation frequency, these velocities were monitored at $x=D$ and $y=0.25D$ aft of the origin. Figure 8, for the sake of brevity, only shows the analysis of the excitation frequency ratios near the limits of the lock-on ranges. At $f_e/f_s = 0.76$ the phase-plane diagram can be seen orbiting in a chaotic path, suggesting the existence of the non lock-on state for this excitation frequency ratio. The corresponding fast Fourier transform (FFT) of the transverse force (F_y) coefficient shows a dominant vortex shedding frequency and a weaker spike occurring at $f_e/f_s = 1$, i.e. the specified excitation frequency. In the range $0.82 \le f_e/f_{s0} \le 1.07$, the phase-plane diagrams exhibit a "limit cycle" and orbiting in a well defined path, indicating the wake has locked onto the forced oscillatory motion. FFT diagrams also confirm this by showing only one single spike at $f_e/f_s = 1$. A typical phase-plane diagram and FFT plot in this lock-on range is shown in Figure 8b. The lock-on range identified here matches that of pure forced transverse oscillation, which also occurs in the range $0.82 \le f_e/f_{s0} \le 1.07$. This implies that in the low excitation frequency ratio range for $\alpha=60°$, the presence of the longitudinal excitation component does not have any effect on the lock-on phenomenon.

Increasing the excitation frequency ratio further, the chaotic non lock-on state reappears and persists up to $f_e/f_s = 1.76$. Figure 8c shows the FFT plot now has the higher peak at the excitation frequency, while the dominant vortex shedding frequency has a smaller peak. From $f_e/f_s = 1.83$ to $f_e/f_s = 2.08$, again phase-plane diagrams show stable trajectories, hence lock-on is achieved within this region. Unlike FFT plots for longitudinal forced oscillations (not shown), where a superposition of one single spike occurs for the lock-on states, the current FFT plots for 60° oscillations show one spike at $f_e/f_s = 1$ and one at $f_e/f_s = 0.5$, as seen in Figure 8d. The reason for this will be further discussed later. The weaker spike at $f_e/f_s = 0.5$ corresponds to the vortex shedding frequency i.e. $f/f_e = f_s/f_e = 0.5$ or $f_e/f_s = 2$, which is the condition at lock-on for pure longitudinal forced oscillations [15]. At $f_e/f_{s0} = 2.14$, the phase-plane diagram shows chaotic behaviour, hence lock-on is not achieved. For higher excitation frequency ratios ($f_e/f_{s0} \ge 3$) a synchronised vortex shedding mode is observed but complete lock-on does not occur, and the phase-plane diagrams (Figure 8e&f)) exhibit quasi-stable trajectories.

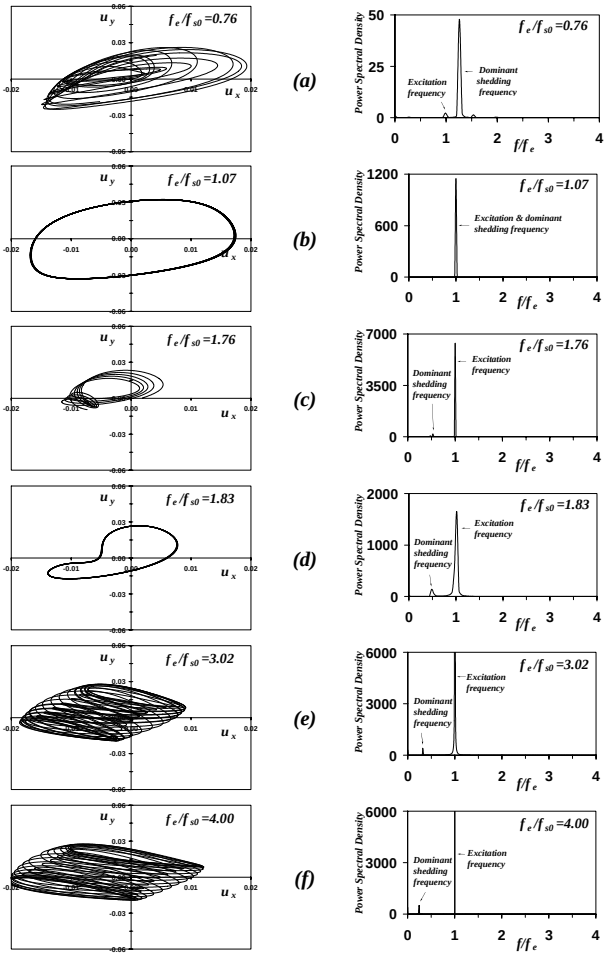

Figure 8 – Phase plane diagrams and fast Fourier transforms of the transverse force coefficient (F_y) for 60° oscillations, *Re=80* and *A/D=0.14*.

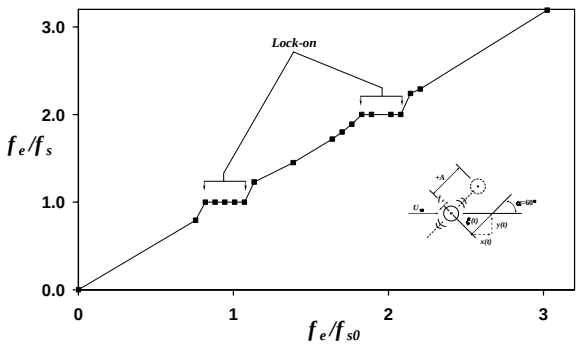

Figure 9 – Summary of two lock-on regions for forced oscillations at 60° with respect to the oncoming flow, *Re=80, A/D=0.14.*

Figure 9 provides a summary of the two identified lock-on regions for oscillations at 60° with respect to the oncoming freestream. The second lock-on region at $f_e/f_{s0}=2$, which ranges from $f_e/f_{s0}=1.83$ to $f_e/f_{s0}=2.08$, is observed to be 57% shorter than the lock-on region of the longitudinal forced oscillations. This suggests that the amplitude of the forced vibration has some influence on the lock-on, particularly for longitudinal oscillations. Further, the presence of two lock-on regions for 60° oscillations may have some engineering importance in the structural design process.

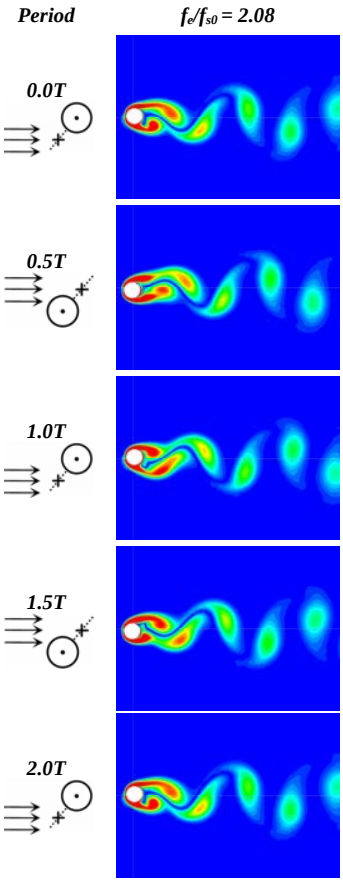

Figure 10 – Vorticity contours for two periods (2T) of 60° oscillations for *Re=80, A/D=0.14*. At 0T, the centre of the cylinder is at the positive extreme position (ξ=+A).

The near wake vortex shedding modes are depicted in Figure 10 for two periods of 60° oscillations at $f_e/f_{s0}=2.08$. At $t=0T$ the centre of the cylinder is at the extreme positive position ($\xi=+A$) as shown in Figure 2. Although not shown here, in the first lock-on range, the near wake exhibits the AI mode for all excitation frequency ratios. Throughout the second lock-on range, the current computation revealed a 2S-per-2T or the equivalent AII mode shown in Figure 10. This agrees with the observation made by Öngören & Rockwell [13] for 60° angle oscillations with $\mathrm{Re}=855$, *A/D*=0.13 and at at $f_e/f_{s0}=2$. It is observed that the formation length of the vortices shed on the upper side is longer compared to the AII mode in the longitudinal oscillation case.

The temporal history of the longitudinal and transverse force coefficients is shown in Figure 11. It can be seen that increasing the excitation frequency ratio results in larger peak-to-peak amplitudes for both force coefficients. For non lock-on states the fluctuation of the transverse coefficient is non-uniform (Figure 11a). For lock-on states, Figure 11b&c, the transverse force coefficient displays a highly organised behaviour. This has been noted by Patnaik *et al.* [14] and it is also another method to reconfirm the lock-on states.

It is further observed that the transverse force coefficient history of 60° oscillations in the first lock-on range (Figure 11b) is different from that in the second lock-on range (Figure 11c). In Figure 11c the transverse force coefficient displays a periodic phenomenon of a high magnitude crest followed by a smaller magnitude crest. The smaller magnitude crest is due to the cylinder's motion on-course to its extreme displacement amplitude ($\xi=\pm A$). Since the oscillations are at an angle of 60° with respect to the freestream, this incidence together with the

speed of the cylinder induces an additional transverse force on the cylinder. This effect can be clearly seen in Figure 12, where the smaller magnitude crests of C_y occur in phase with when the cylinder is at maximum displacement. The higher magnitude crests are due to the superposition of the cylinder moving to its extreme displacement amplitudes and the simultaneous occurrence of the shedding of a vortex. Since this is the second lock-on region, where $f_e = 2f_s$, superposition occurs every second excitation period.

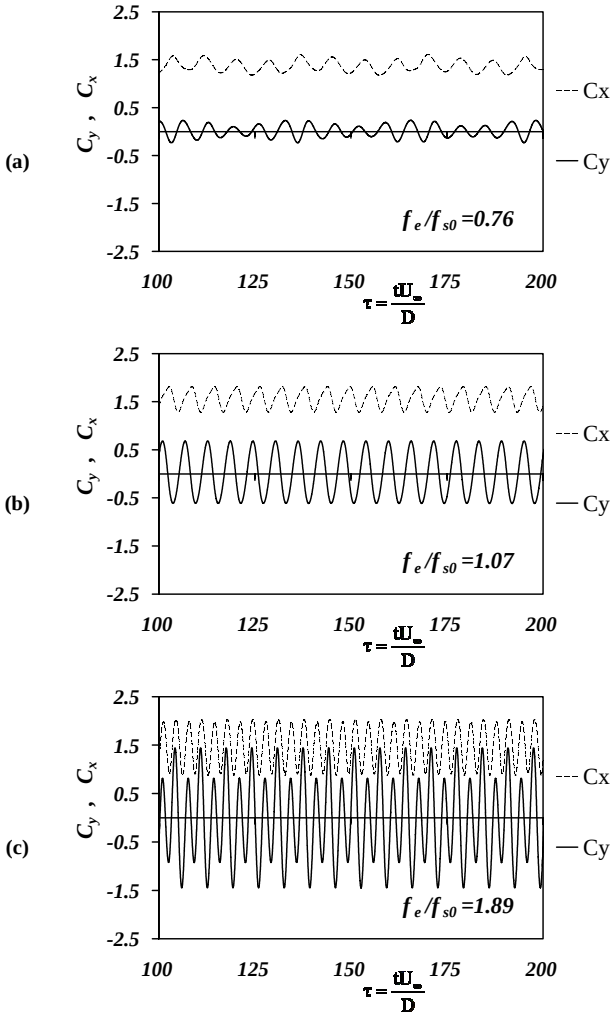

Figure 11 – Variations of transverse and longitudinal force coefficients for 60° oscillations.

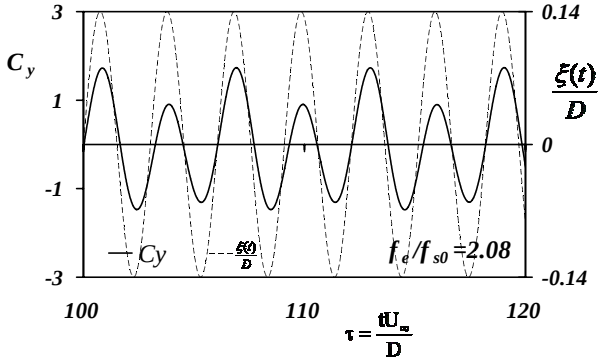

Figure 12 – Transverse force coefficient history and displacement trajectory of 60° forced oscillations, *Re*=80, *A/D*=0.14.

Consequently, the earlier FFT plots of Figure 8d exhibits two distinct peaks as opposed to the superimposed single peak often seen at the lock-on condition of Figure 8b. Further, the effect of periodic high magnitude crest followed by a smaller magnitude crest is not seen in Figure 11b, because the shedding of vortices is synchronised to every period of oscillation $f_e / f_s = 1$.

Figure 13 shows the average and fluctuating force coefficients across the excitation frequency ratio range. It can be seen that the mean longitudinal force coefficient exhibits two amplification "humps", reflecting the lock-on regions identified in Figure 9. It is interesting to note that in the second lock-on range, although the excitation frequency is much higher, the longitudinal force amplification is of the same magnitude as that of the first lock-on range. The fluctuations of the transverse force coefficient, on the other hand, exhibit significant increase with excitation frequency ratio. This is due to a combination of the 60° angle of attack and the increase in excitation frequency (hence speed) of the circular cylinder generating additional fluctuating transverse force.

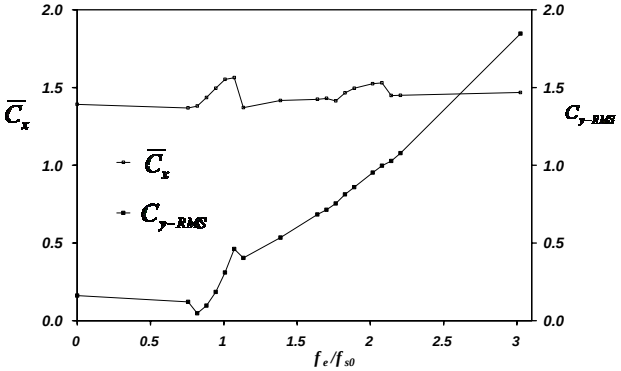

Figure 13 – Mean and fluctuating force coefficients for 60° forced oscillations, *Re*=80, *A/D*=0.14.

When the amplitude ratio is increased up to 0.5D for 60° forced oscillations, the entire wake street behind the circular cylinder exhibits a deviated effect from zero mean oscillating plane, *y*=0. It is known that a von Karman street normally has an axis of asymmetry that runs parallel to the in-coming flow through the centre of the circular cylinder. The same holds true for a cylinder undergoing oscillations in the transverse and longitudinal directions, exhibiting different modes of vortex shedding. In these cases the axis of asymmetry (for antisymmetrical vortex shedding modes) or axis of symmetry (symmetrical modes) still runs parallel to the mean oscillating position. From the current computations with high amplitude oscillations, it is observed that a synchronised AI mode wake is deviated from the line y=0 when the excitation frequency is within the first lock-on range as shown in Figure 14. The direction of deviation depends on whether the angle of oscillation is positive or negative. This effect possibly has some engineering implications in flow control situations where the vortices can be induced to shed away from a trailing structure.

Conclusions

Laminar incompressible flow past a circular cylinder forced to oscillate longitudinally, transversely and at a 60° angle to the uniform freestream is simulated using the dynamic mesh method. This method presents a powerful approach in simulating a moving body in the presence of other structures. Extensive validation of the simulation results has yielded good agreement with the available experimental and numerical data.

When the circular cylinder is forced to oscillate at 60° to the uniform freestream, two lock-on regions are identified. This has been confirmed with various analysis techniques such as phase-

plane diagrams, FFT plots, time history behaviour of the transverse force coefficient, and the locations of average longitudinal force coefficient amplifications. The first lock-on occurs within $0.82 \le f_e / f_{s0} \le 1.07$, while the second lock-on takes place in the range $1.83 \le f_e / f_{s0} \le 2.08$, for $\mathrm{Re} = 80$ and *A/D*=0.14. The first lock-on is the same as that when the oscillation is in the pure transverse direction, while the second lock-on region is 57% shorter compared to that of the longitudinal excitation only. This suggests that the longitudinal excitation component in the 60° angle oscillations has minimal effect on the locking-on phenomena. Vortex shedding modes AI and AII are observed at the first and second synchronised states respectively, agreeing with the observation made by an experimental study with the same oscillation configuration but different Reynolds number and amplitude ratio. At higher amplitude oscillations, the wake street consistently displays a deviation effect from the centreline, with the direction of deviation depending on the direction of moving cylinder.

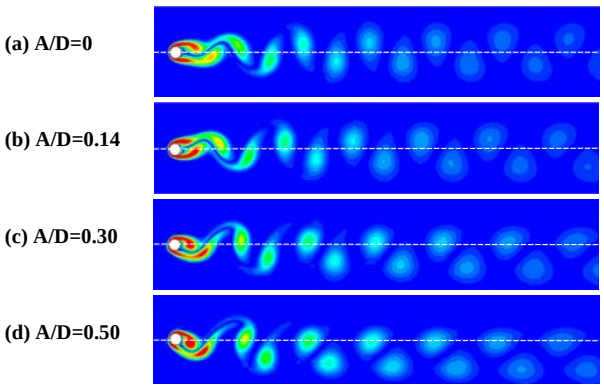

Figure 14 – Deviation of AI mode wake street at higher amplitude ratios compared to the case with cylinder at rest (A/D=0). *Re*=80 and f_e/f_{s0}=0.95.

Acknowledgments

This work was supported by Australian Postgraduate Awards (APA) from the Australian Government and the School of Aerospace, Mechanical and Manufacturing Engineering at RMIT University and Defence Science & Technology Organisation, Australia,.

References

[1] Al-Mdallal, Q., *et al.* Forced streamwise oscillations of a circular cylinder: Locked-on modes and resulting fluid forces. *Journal of Fluids and Structures* (2007) doi:10.1016/j.jfluidsstructs.2006.11.001.

[2] Bishop, R.E.D., Hassan, A.Y., 1964a. The lift and drag forces on a circular cylinder oscillating in a flowing fluid. *Proceedings of Royal Society (London) A*, **277**, 51-75.

[3] Bishop, R.E.D., Hassan, A.Y., 1964b. The lift and drag forces on a circular cylinder in a flowing fluid. *Proceedings of Royal Society (London) A* **277**, 32-50.

[4] Blackburn, H.M., Henderson R.D., 1999. A study of two-dimensional flow past an oscillating cylinder. *Journal of Fluid Mechanics*, **385**, 225-286.

[5] Braza, M., Chassaing, P. & Ha Minh, H., 1986, Numerical study and physical analysis of the pressure and velocity fields in the near wake of a circular cylinder. *Journal of Fluid Mechanics*, **165**, 79.

[6] Englman, M.S. & Jamnia, M.A. 1990. Transient flow past a circular ylinder: a benchmark solution. *Intl. J. Numer. Methods Fluids.* **11**, 985

[7] Karniadakis, G., Triantafyllou, G., 1989. Frequency selection and asymptotic states in laminar wakes. *Journal of Fluid Mechanics*, **199**, 441-469.

[8] King, R., 1977, A review of vortex shedding research and its application. *Ocean Engineering*, **4**, 141-172.

[9] Koopman, G.H., 1967. The vortex wakes of vibrating cylinders at low Reynolds numbers. *Journal of Fluid Mechanics*, **28**, 501-512.

[10] Griffin, O.M., Ramberg, S.E., 1974. The vortex-street wakes of vibrating cylinders. *Journal of Fluid Mechanics*, **66**, 553-576.

[11] Li, J., Sun, J., Roux, B., 1992. Numerical study of an oscillating cylinder in uniform flow and in the wake of an upstream cylinder. *Journal of Fluid Mechanics*, **237,** 457-478.

[12] Naudascher, E., 1987. Flow-induced streamwise vibrations of structures. *Journal of Fluids and Structures*, **1**, 257-271.

[13] Öngören, A., Rockwell, D., 1987. Flow structure from an oscillating cylinder Part 2. Mode competition in the near wake. *Journal of Fluids Mechanics*, **191**, 225-245.

[14] Patnaik, B.S.V., Narayana, P.A.A., Seetharamu, K.N., 1999. Numerical simulation of laminar flow past a transversely vibrating circular cylinder. *Journal of Sound and Vibration*, **228**, 459-475.

[15] Tanida, Y., Okajima, A., Watanabe, Y., 1973, Stability of a circular cylinder oscillating in uniform flow or in a wake. *Journal of Fluid Mechanics*, **61**, 769-784.

[16] Tritton, D.J., 1971, A note on vortex streets behind circular cylinders at low Reynolds numbers. *Journal of Fluid Mechanics*, **45**, 203.

[17] Williamson, C.H.K., Roshko, A., 1988. Vortex formation in the wake of an oscillating cylinder. *Journal of Fluids and Structures* **2**, 355-381.